Applied Clay Science xxx (2016) xxx–xxx

Contents lists available at ScienceDirect

Applied Clay Science

journal homepage: www.elsevier.com/locate/clay

Research paper

Multi-scale study on the deformation and fracture evolution of clay rock sample subjected to desiccation

Anne-Laure Fauchille [a], Stephen Hedan [a,*], Valéry Valle [b], Dimitri Pret [a], Justo Cabrera [c], Philippe Cosenza [a]

[a] Université de Poitiers, CNRS UMR 7285 IC2MP, HydrASA, Ecole Nationale Supérieure d'Ingénieurs de POITIERS, Bât B27-TSA 51106, 4, rue Michel Brunet, 86073 POITIERS CEDEX 9, France
[b] Université de Poitiers, CNRS UPR 3346 Institut PPRIME, S.P. 2 M.I., Bd. M. et P. Curie, Téléport 2, B.P. 30179, 86962 Futuroscope Chasseneuil Cedex, France
[c] DEI-SARG Department, Institute for Radiological Protection and Nuclear Safety, B.P. 17, 92262, Fontenay-aux-Roses Cedex, France

ARTICLE INFO

Article history:
Received 10 September 2015
Received in revised form 27 January 2016
Accepted 30 January 2016
Available online xxxx

Keywords:
Desiccation cracks
Clay minerals
Hydric strains
Tournemire argillite
Digital image correlation
Multi-scale study

ABSTRACT

The aim of this paper is to compare and discuss the values of strains and crack apertures associated with desiccation cracks measured in Tournemire clay rock at different scales (micrometer to decimeter). Experimental investigations in the laboratory were conducted on one clay rock sample subjected to a desiccation process. Two faces with dimensions of 20 × 20 mm^2 (i.e., macroscopic scale) and 5.1 × 4.1 mm^2 (i.e., mesoscopic scale) were analyzed. The induced hydric strains and desiccation cracking were monitored by digital image correlation combined with a new algorithm (H-DIC). The results were compared with the data of Hedan et al. (2014) at the gallery scale (decimeter) and those of Wang et al. (2013) at the microscopic scale (micrometer).

Our laboratory study yielded the following phenomenological results. First, the displacement fields revealed the presence of sub-horizontal cracks associated with the direction of bedding planes and sub-vertical cracks, as previously observed in a gallery front in Tournemire Station. Second, when the relative humidity (RH) decreased between 98% and 33%, the crack aperture kinematics at the macroscopic scale (centimeter) was divided into three steps: (*i*) a phase of opening and closure, (*ii*) a phase of only gradual closure, and (*iii*) a final phase in which the desiccation cracks closed. Only phases (ii) and (iii) were observed at the mesoscopic scale (millimeter), revealing that the kinematics of cracks depends on the scale observed. The comparison of the strains at the mesoscopic and the macroscopic scales also highlights that their values depend on the study scale: the presence of cracks at the mesoscopic scale leads to a large overestimation of the values of the strains calculated at the macroscopic scale. In contrast to the observations in the laboratory, the desiccation cracks detected in the gallery systematically open when RH decreases. This difference and the differences observed in the geometrical organization of crack networks are explained by the different boundary conditions prevailing in both cases (i.e., free swelling/shrinkage in laboratory versus constrained swelling/shrinkage in the gallery).

The interpretation of the entire dataset emphasizes the need for a multi-scale approach to understand and model desiccation cracking mechanisms and the associated hydric strains in clay rocks.

List of symbols

f	gray-level function
g	gray-level function
u	displacement in x direction
v	displacement in y direction
w	displacement in z direction
CF	correlation function
D	interval between two centers of subset
N	number of pairs of independent displacement measurements
RH	relative humidity
T	temperature
ΔW	averaged water content
d_n^c	mean aperture values
c	type of crack
n	number of cracks
ε_{is_sample}	in-plane mean strain as a qualitative indicator of the average volume variation of the sample
ε_{is_macro}	in-plane mean strain as a qualitative indicator of the average volume variation of the solid phase at the macroscopic scale
ε_{is_meso}	in-plane mean strain as a qualitative indicator of the average volume variation of the solid phase at the mesoscopic scale
ε_1	major principal strain
ε_2	minor principal strain
σ_{ui}	displacement standard deviation

* Corresponding author.
E-mail address: stephen.hedan@univ-poitiers.fr (S. Hedan).

http://dx.doi.org/10.1016/j.clay.2016.01.054
0169-1317/

1. Introduction

Clay rocks have been considered as potential repositories for high-level radioactive wastes in several industrial countries. Among the critical issues related to the long-term safety assessment of such geological repositories, the study of the so-called excavation damaged zone (EDZ) is particularly important. The initiation and extension of the EDZ are governed by many parameters (Bossard et al., 2002; Tsang et al., 2005; Blüming et al., 2007) including the material properties of the rock, such as the material anisotropy; the initial stress field; the existence of natural fracture zones in the rock mass; the geometry of the gallery; and the hydric state in the gallery. With regard to the hydric state in the gallery, fractures associated with the desaturation of argillaceous medium have been observed on gallery fronts in several underground research laboratories, such as the experimental platform of Tournemire (Cabrera et al., 2001; Matray et al., 2007) and the Mont Terri Laboratory (Möri et al., 2010). This hydric fracturing process is evidenced in situ by sub-horizontal cracks spaced at several decimeters on all vertical walls in contact with ambient air. In winter (dry state), the corresponding crack apertures can reach a few millimeters, whereas these cracks are closed in summer (wet state). These sub-horizontal cracks induced by desiccation are parallel to the bedding planes, suggesting that they are partially controlled by sedimentological patterns (e.g., vertical differences in sediment grain size and mineral composition or organization). Recent studies have revealed other types of sub-horizontal desiccation cracks (Hedan et al., 2014; Valle et al., 2015) with a distance of approximately 64–100 mm and sub-vertical cracks (Hedan et al., 2014) connected to the sub-horizontal cracks with features identical to those of the sub-horizontal cracks. These observations of clay rock damage induced by drying have been obtained in the field using the digital image correlation (DIC) technique. At a much lower scale, Wang et al. (2013, 2014) applied the DIC algorithm directly on back-scattered electron images ($128 \times 111\ \mu m^2$) from an environmental scanning electron microscope (ESEM). By means of this combination of ESEM and DIC techniques, the swelling/shrinkage and more generally the hydromechanical behavior of the Callovo-Oxfordian clay rock located in the Paris basin was investigated at the micrometer scale. Their observations revealed two micromechanisms. First, the local swelling or shrinkage is strongly anisotropic in the plane perpendicular to the bedding planes (with the major swelling direction normal to the bedding plane). Second, a complex network of microcracks with typical openings of approximately 1 μm was detected in both the wetting and drying paths. These microcracks were located in the bulk of the clay matrix and/or at quartz/carbonate inclusion–clay matrix interfaces (Wang et al., 2014).

However, these previous observations were all obtained at very different space scales, and the phenomenological links or causal relationships between them are unclear. The relationships between these observations acquired at different scales could facilitate the identification of the micromechanisms governing desiccation cracking.

Following this perspective, the main objective of this laboratory investigation was to design an original methodology for providing new observations and correlations between hydric strains, desiccation crack apertures and state variables (relative humidity (RH) and water content) at the millimeter and centimeter scales. These scales are rarely investigated in the context of clay rocks. This methodology is based on the combination of a new experimental setup and a new DIC algorithm (H-DIC). On the same sample, this combination allows the measurement of the kinematic field and patterns for the two considered scales (i.e., millimeter and centimeter scales). The results were compared with those previously obtained at the micrometer and gallery scales to provide physical constraints to improve the models and the understanding of desiccation cracking in clay rocks.

2. Geological setting and sampling

The clay rock sample we studied came from the Tournemire Underground Research Laboratory (URL) of the Institute for Radioprotection and Nuclear Safety (IRSN) in Aveyron, France. The Tournemire URL was excavated in a sub-horizontal consolidated argillaceous Toarcian formation (250 m thick) with marly layers (50 m thick) from the Domerian age, which compose a part of the Mesozoic basin located on the southern border of the French Massif Central (Bonin, 1998; Cabrera et al., 2001; Constantin et al., 2002). The sample comes from the upper Toarcian, corresponding to a 160-m-thick layer of argillite.

The mineralogical composition of the upper Toarcian formation shows that clay minerals (kaolinite, illite, and illite/smectite mixed-layer minerals) represent approximately 40 wt.% of the bulk-rock composition. The clay fraction is mainly composed of illite (5–15 wt.%), illite/smectite mixed-layer minerals (5–10 wt.%), chlorite (1–5 wt.%), and kaolinite (15–20 wt.%). The Tournemire argillite also contains 10–20 wt.% of quartz grains, 10–40 wt.% of carbonates (mainly calcite), and 2–7 wt.% of pyrite (Bonin, 1998; De Windt et al., 1998; Cabrera et al., 2001; Charpentier et al., 2004; Tremosa et al., 2012). The water content is between 3.5 and 4.0 wt.%.

Geomechanical investigations (Niandou et al., 1997; Cosenza et al., 2002) have demonstrated that Tournemire argillite is a transverse isotropic geomaterial.

Three different types of cracks are observed at the Tournemire experimental station (Cabrera et al., 2001; Matray et al., 2007; Okay et al., 2013):

(i) fractures in the gallery walls induced by stress redistribution during excavation (millimeter-scale width and meter-scale extension);
(ii) pre-existing tectonic fractures in the rock mass (same dimensions as the previous fractures, i.e., mm-scale width and m-scale extension); and
(iii) networks of regularly spaced (at approximately 20 cm) sub-horizontal cracks parallel to the bedding planes. These sub-horizontal cracks, which are easily observed on the vertical walls of the Tournemire galleries, are each several decimeters deep with sub-millimeter apertures.

The set of sub-horizontal cracks is directly linked to seasonal variations in atmospheric properties (hygrometry and temperature) at the Tournemire experimental station and results from variations in the chemical potential of the interstitial solutions under wetting/drying cycles (Cabrera et al., 2001; Valès et al., 2004; Hedan et al., 2014).

The experimental investigation that focused on these cracks used a small sample ($2 \times 2 \times 2\ cm^3$) of argillite core in an undisturbed state (i.e., taken far from the EDZ). The distance between the gallery wall and sample was 4.2 m (Fig. 1). The disturbed zone is up to 1.5 m deep (Matray et al., 2007), and thus the sample was taken from an undisturbed area. The drilling was performed with air to avoid any contact of the formation with any type of aqueous solution. After drilling, the core was immediately placed in an Al-coated plastic bag and removed from the FD90 borehole, which was drilled in 2010 perpendicular to the wall of the north gallery of the Tournemire URL. The FD90 borehole is sub-horizontal and parallel to the bedding planes (Fig. 1).

3. Experimental set-up and methods

3.1. Experimental set-up

The experimental set-up comprised a plastic waterproof box (Fig. 2a) in which the humidity and temperature conditions were controlled. RH was controlled by saline solutions, and the temperature

Please cite this article as: Fauchille, A.-L., et al., Multi-scale study on the deformation and fracture evolution of clay rock sample subjected to desiccation, Appl. Clay Sci. (2016), http://dx.doi.org/10.1016/j.clay.2016.01.054

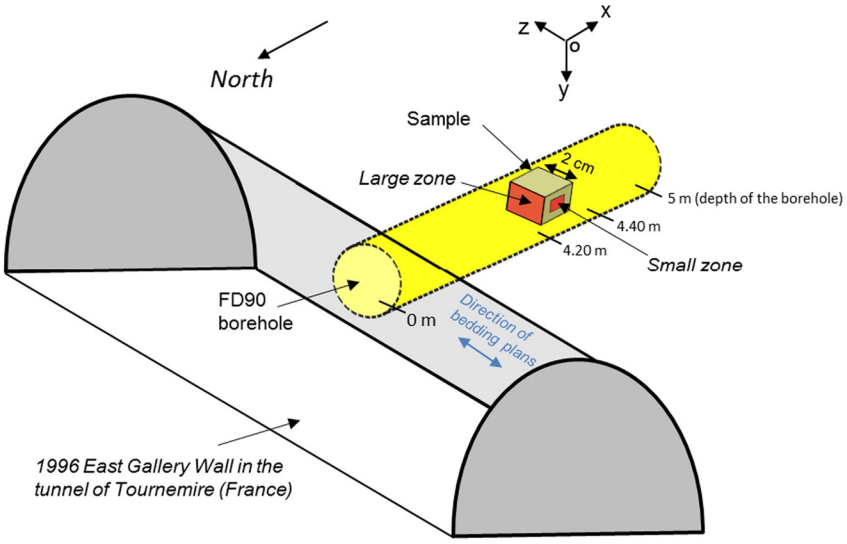

Fig. 1. Location and orientation of the sample in the FD90 borehole in the URL of Tournemire, France.

was controlled by an air-conditioning unit at 22 ± 1 °C. The box contained an RH/T sensor (Testo© 175H1, with a precision of ±2% and 0.3 °C for the RH and temperature, respectively), a precision balance (ADAM© PGW 753e; precision of ±0.002 g) and a stirred saline solution. The solution was stirred with a programmable electric plug for 2 min every 15 min to preserve a constant temperature. Two cameras with a resolution of 5 Mp (2560 × 1920 pixels) acquired images (0.5 image·min^{-1}) with a spatial resolution of 2.2 µm·pixel^{-1} for the smaller zone (i.e., millimeter scale, hereafter referred to as the mesoscopic scale) and 10 µm·pixel^{-1} for the larger zone (i.e., centimeter scale, hereafter referred to as the macroscopic scale). These two zones were on two different sample faces (Fig. 2b). In clay rocks, the clay matrix and the coarse grains are visible at the mesoscopic scale but appear homogeneous at the macroscopic scale (Robinet, 2008). A 400-W lamp lit the sample when the camera acquired images. To avoid heating induced by the lamp, the lamps were computer programmed to turn on only when the camera acquired a picture. The sample was saturated at RH of 98% before desaturation and was submitted to desiccation from 98% to 33% RH. The RH values of 98% and 33% correspond to similar extreme RH values observed in the tunnel of Tournemire (from 100% to 30%). The evolution of the RH inside the box is presented in Fig. 3. After desaturation from 100 to 33% RH, the sample was subjected to further desiccation at 5% RH with a saline solution of P_2O_5 in the waterproof box. The water content ΔW calculated in this paper is relative to the mass of the dry state at 5% RH. Oven drying was not possible because the sample was directly reused for scanning electron microscopy analysis (Fauchille et al., 2014; Fauchille, 2015).

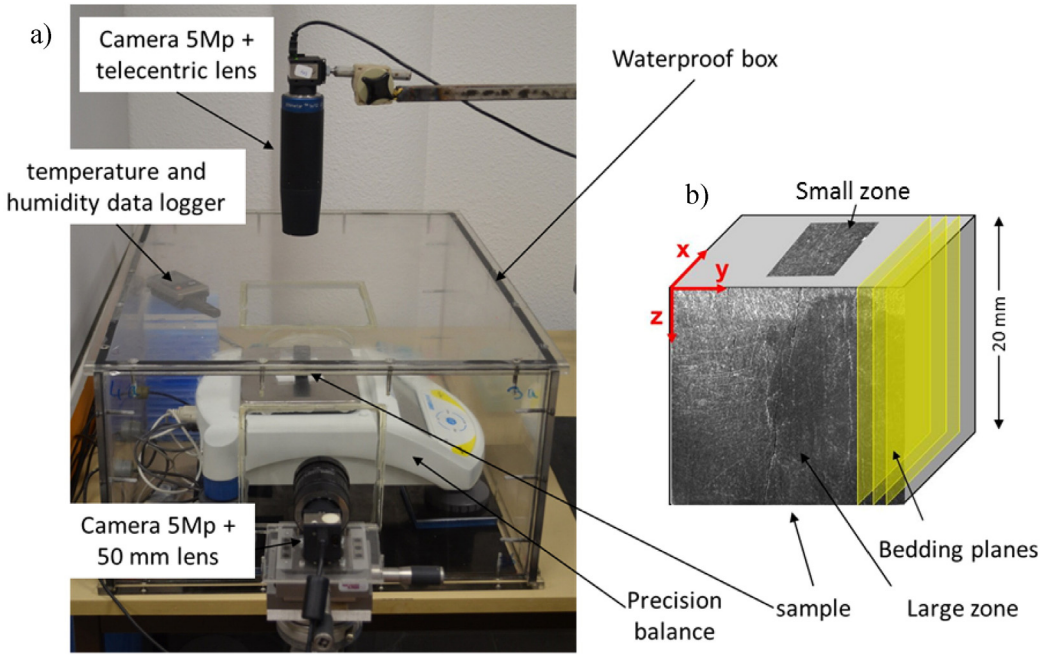

Fig. 2. a) Experimental set-up and b) location of the large and small zones on the sample.

Please cite this article as: Fauchille, A.-L., et al., Multi-scale study on the deformation and fracture evolution of clay rock sample subjected to desiccation, Appl. Clay Sci. (2016), http://dx.doi.org/10.1016/j.clay.2016.01.054

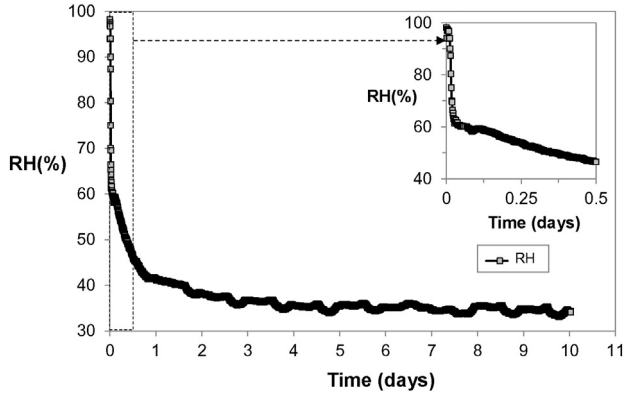

Fig. 3. Variation of RH versus time (days).

The advantage and novelty of this setup compared to previous studies are its ability to measure kinematic parameters on the same sample at two different spatial scales (in this case, the millimeter and centimeter scales).

3.2. Digital image correlation method

In geomechanics, the DIC technique (Sutton et al., 1983; Bruck et al., 1989) has been successfully used to observe strain localization in geomaterials (Desrues et al., 1985), detect crack positions and calculate crack openings in clay rocks (Hedan et al., 2012, 2014; Wang et al., 2013, 2014). The DIC technique has been used under various loadings (Bésuelle et al., 2006; Lenoir et al., 2007; Bornert et al., 2010; Yang et al., 2011).

To obtain the displacement field of an area undergoing mechanical transformation, the DIC method monitors the positional changes of a speckle pattern located on the sample surface. The speckle pattern is typically artificial to ensure adequate variations of contrast between images, but in this study, the speckle was the natural surface of the sample. The sample obtained had adequate speckle at the macroscopic scale. At the mesoscopic scale, the speckle was obtained by polishing the sample with silicon carbide and diamond products without epoxy resin (Fauchille, 2015).

Two images are necessary to obtain the full-field in-plane displacements; the first gray-level function $f(x, y)$ is acquired at the initial state t_0, and the second gray-level function $g(x^*,y^*)$ is acquired at an actual state t. The principle of this method is to minimize the correlation function between the functions f and g for a given subset S (Sutton et al., 1983; Bruck et al., 1989). Several DIC methods have been developed to determine the precise kinematic field (u, v) in the area of a crack and evaluate its position (Jin and Bruck, 2005; Réthoré et al., 2008; Grégoire et al., 2009).

In this study, H-DIC software (Heaviside-based DIC) was employed (Valle et al., 2015). This software is based on an extension of the classic DIC method enriched by adding two-dimensional Heaviside functions $H(x, y)$ using a local approach and minimization process on a subset. This algorithm enables the crack location (discontinuities of displacement) to be determined with a precision of ± 1 pixel. The reader is referred to Valle et al. (2015) for more details.

In this study, all images contained 2560×1920 pixels. For the small and large zones, the magnifications were 2.2 and 10 $\mu m \cdot pixel^{-1}$, respectively. The subset size was 64×64 pixels (i.e., 140.8×140.8 μm^2 for the small zone and 640×640 μm^2 for the large zone), and the increment between two calculations was $D = 1$ pixel. The bi-cubic image interpolation algorithm was used for sub-pixel evaluation.

3.2.1. Crack aperture

A crack position is characterized by a discontinuity of displacement on the displacement fields (Valle et al., 2015). The crack apertures are typically calculated by subtracting both displacement values normal to the crack faces. In our case, these normal displacements are actually extrema of the displacement values around the crack. Moreover, the calculated aperture values displayed in this section are always positive because all of the images were compared to the reference image corresponding to closed cracks. Indeed, the reference image is the last image taken during the test. Moreover, an increase in the calculated aperture corresponds to crack opening, whereas a decrease in the crack aperture is associated with crack closure.

The mean aperture values d_n (n is the crack number) were calculated by subtracting the extrema of displacements (u and v for the small zone, and v and w for the large zone) on both sides of the crack and averaging this subtraction over all subsets defining the "crack":

$$d_n = \frac{1}{N}\sum_{N}\sqrt{(u_n(x,y)-u_n(x+var1,y+var2))^2+(v_n(x,y)-v_n(x+var1,y+var2))^2} \quad (1)$$

N is the number of subsets defining each "crack", $u_n(x, y)$ and $u_n(x + var1, y + var2)$ are the extrema of the u displacements on both sides of the crack n, and $v_n(x,y)$ and $v_n(x+var1,y+var2)$ are the extrema of the v displacements on both sides of the crack n. $var1$ and $var2$ define the distances in the x and y directions, respectively, to find the highest aperture in the area. The range $var1$ is 1–5 pixels, and $var2$ is 1–3 pixels. The calculation was performed in small rectangular areas of 5×3 pixels, including the crack. Other area sizes were tested (2×1, 4×1, 2×2 and 3×3 pixels) (Fauchille, 2015), but 5×3 pixels was optimal for calculating the aperture locally while searching for the highest aperture. This calculation was independent of the crack orientation versus the camera coordinate system and accounts for an aperture in opening mode (mode I) and an aperture in shear mode (mode II).

In contrast to the displacements, the values of d_n are not affected by the rigid-body movements of the camera.

3.2.2. In-plane strains

The strain ε_{is_sample} is the average in-plane strain, which corresponds to the measured strain at the sample scale in the large zone (20×20 mm^2). ε_{is_sample} is the sum of the in-plane principal strains ε_1 and ε_2 calculated on the same sample face:

$$\varepsilon_{is}(x,y) = \varepsilon_1(x,y) + \varepsilon_2(x,y) \quad (2)$$

The calculation is performed by measuring the variable distances between natural markers on the sample borders of the large zone (Fig. 2) during the desiccation process. The location of the centers of the markers was measured using the mark-tracking method (Rotinat et al., 2001). The ε_{is_sample} sample includes all cracks in the large zone and the sample deformation. This is a qualitative "volumetric" strain (Wang, 2012) because the Tournemire clay rock is considered a transversely isotropic material. This value can also be obtained with a displacement sensor (Valès, 2008).

The strain ε_{is_macro} is an average of each $\varepsilon_{is}(x,y)$ (Eq. 5) inside an area of 250×250 pixels in the large zone (macroscopic scale) without cracking, and the strain ε_{is_meso} was measured in an area of 200×200 pixels in the small zone (mesoscopic scale) without cracking. The zones selected to calculate ε_{is_macro} and ε_{is_meso} were those in which the noise was lowest and no cracks were detected.

4. Results

4.1. Types of cracks

For the large zone, the maps in Fig. 4a and b correspond to the w-displacement along the z-axis and the v-displacement along the y-axis. For the small zone, the maps in Fig. 4c and d correspond to the

Please cite this article as: Fauchille, A.-L., et al., Multi-scale study on the deformation and fracture evolution of clay rock sample subjected to desiccation, Appl. Clay Sci. (2016), http://dx.doi.org/10.1016/j.clay.2016.01.054

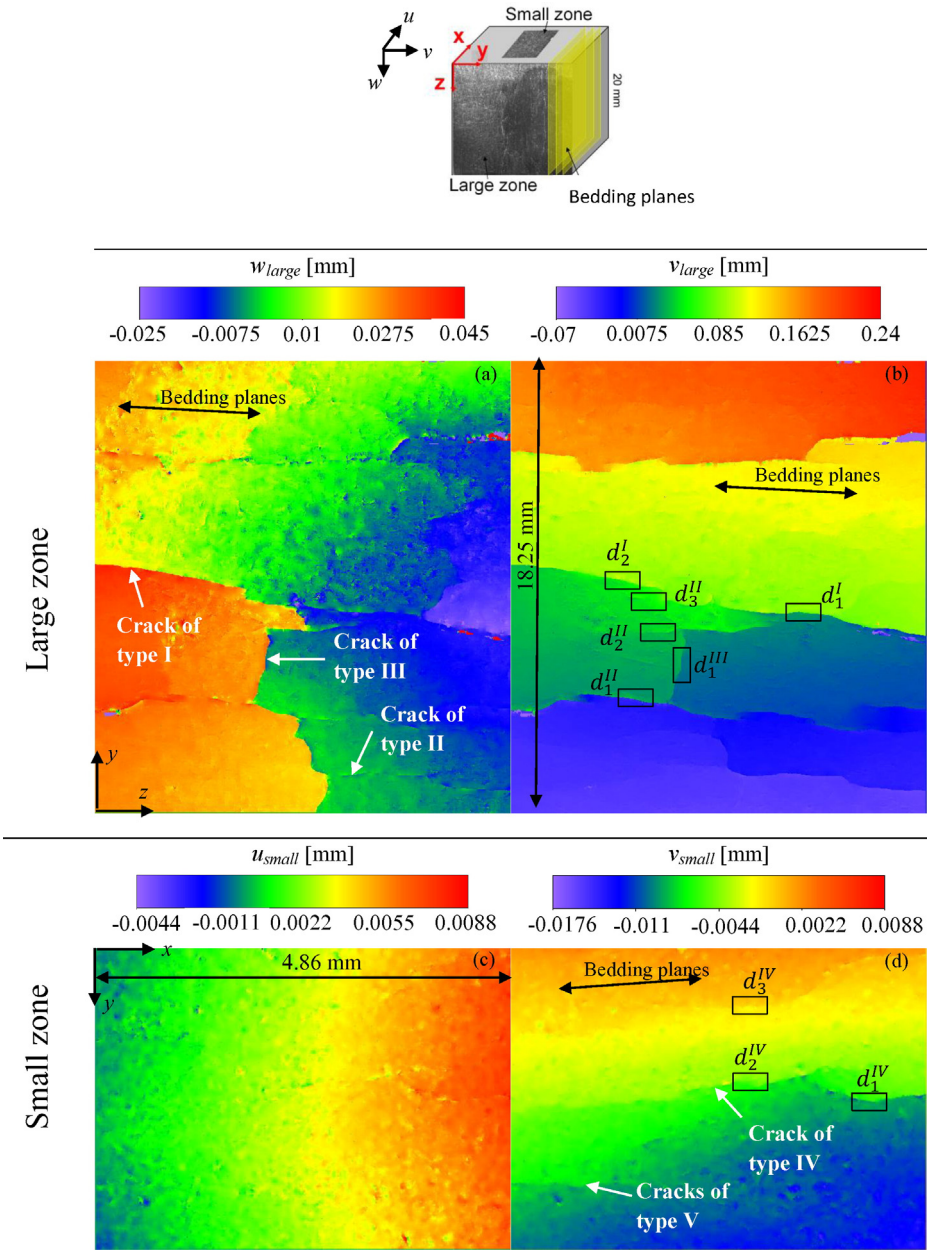

Fig. 4. Displacement fields (u,v,w) in mm obtained from the H-DIC algorithm for the large and small zones.

u-displacement along the x-axis and the v-displacement along the y-axis, respectively.

The in-plane horizontal displacements $u(x,y)$ and $w(x,y)$ were parallel to the bedding planes, whereas the in-plane vertical displacements $v(x,y)$ were perpendicular to the bedding planes.

The significant local variations of color on v and w indicate discontinuities of displacement and the presence of desiccation cracks (Fig. 4a–d). Moreover, the maps show the presence of sub-horizontal and sub-vertical cracks, as observed in the in situ investigation on the gallery front (Hedan et al., 2014).

For the large zone, the displacement fields (v, w) defined three types of desiccation cracks (Fig. 4 a, b):

- Type I: parallel to the bedding planes (sub-horizontal) and crossing the large zone.
- Type II: parallel to the bedding planes (sub-horizontal) and not crossing the large zone.
- Type III: perpendicular to the bedding planes (sub-vertical) and connected to the sub-horizontal crack in the large zone.

For the small zone, the v-displacement field defined two types of desiccation cracks (Fig. 4d):

- Type IV: parallel to the bedding planes (sub-horizontal) and crossing the small zone.
- Type V: parallel to the bedding planes (sub-horizontal) and not crossing the small zone.

In Fig. 4c, the u-displacement field for the small zone did not detect any crack at the investigated scale (1 pixel = 2.2 μm). This field exhibited a constant slope of displacement. In the studied zones, some displacement discontinuities were observed for the large and small zones (Fig. 4a–d). These displacement maps enabled the monitoring of the

Please cite this article as: Fauchille, A.-L., et al., Multi-scale study on the deformation and fracture evolution of clay rock sample subjected to desiccation, Appl. Clay Sci. (2016), http://dx.doi.org/10.1016/j.clay.2016.01.054

crack apertures and in-plane mean strain with respect to time, RH and ΔW.

4.2. Evolution of the crack apertures during desiccation

There were five types of cracks; the crack aperture is written as d_n^c, where c is the type of crack (between I and V) and n is the crack number. The average crack apertures for different cracks were calculated in small areas containing 50 to 70 pixels of one crack (black areas in Fig. 4b and d) to compare their evolution during the desiccation process (Fig. 5). The results shown in Figs. 5a to 6d were associated with the eight sub-horizontal desiccation cracks (d_1^I, d_2^I, d_1^{II}, d_2^{II}, d_3^{II}, d_1^{IV}, d_2^{IV}, and d_3^{IV}) and one sub-vertical crack (d_1^{III}) that were visible at the beginning of the test. The reference image (t_0) acquired at the end of data acquisition (closed cracks) was considered, and the time indicated in Fig. 5 corresponds to the time between the beginning of the study and the acquisition of the recorded images.

The closure of the desiccation cracks was effective during desiccation (Fig. 5a to d).

The maximum apertures for the eight sub-horizontal cracks at the beginning of the test exhibited values in the range of 1.3 to 3.5 μm for the small zone (d_1^{IV}, d_2^{IV}, and d_3^{IV}) and 12 to 58 μm for the large zone (d_1^I, d_2^I, d_1^{II}, d_2^{II}, d_3^{II}). The crack aperture of the sub-vertical crack (d_1^{III}) was on the same order of magnitude as those of the sub-horizontal cracks.

The evolution of the cracks can be divided into three steps (Fig. 5a to d):

- In the first step, an opening of type I and III cracks in the large zone was measured (Fig. 5a) and confirmed by a positive crack opening velocity (Fig. 5b). Simultaneously, a closure of cracks of type II (large zone) and IV (small zone) was measured and confirmed by negative values of the crack opening velocity (Fig. 5b and d). Moreover, two cracks of type IV (d_2^{IV}, d_3^{IV}) had nearly null opening velocities at the beginning of step 1, contrary to crack IV d_1^{IV}. Thus, crack d_1^{IV}started to close before the two others cracks of type IV (Fig. 5d).
- In the second step, closure of all desiccation cracks was measured in the large and small zones (Fig. 5a and c), and confirmed by the negative crack opening velocities (Fig. 5b and d).
- In the third step, the desiccation cracks were closed, and the crack opening velocities were nearly zero.

The type IV cracks did not correspond to part of the type I or II cracks because the amplitude of the crack aperture was significantly different (the maximum of d_1^{IV} is 3.5 μm, and the maximum of d_1^I or d_1^{II} is between

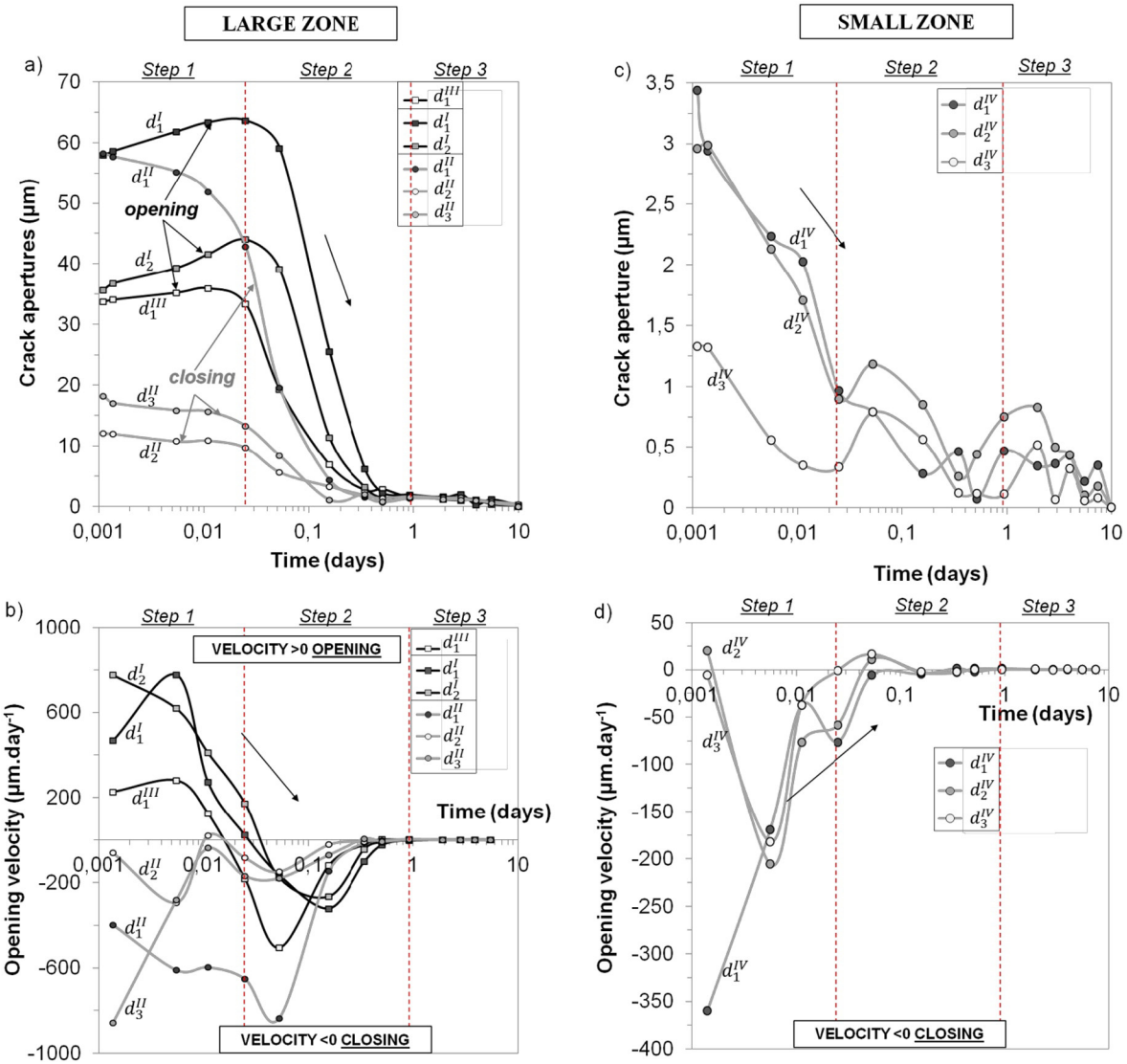

Fig. 5. For the large zone: a) crack aperture and b) opening velocity vs time; for the small zone: c) crack aperture and d) opening velocity vs time.

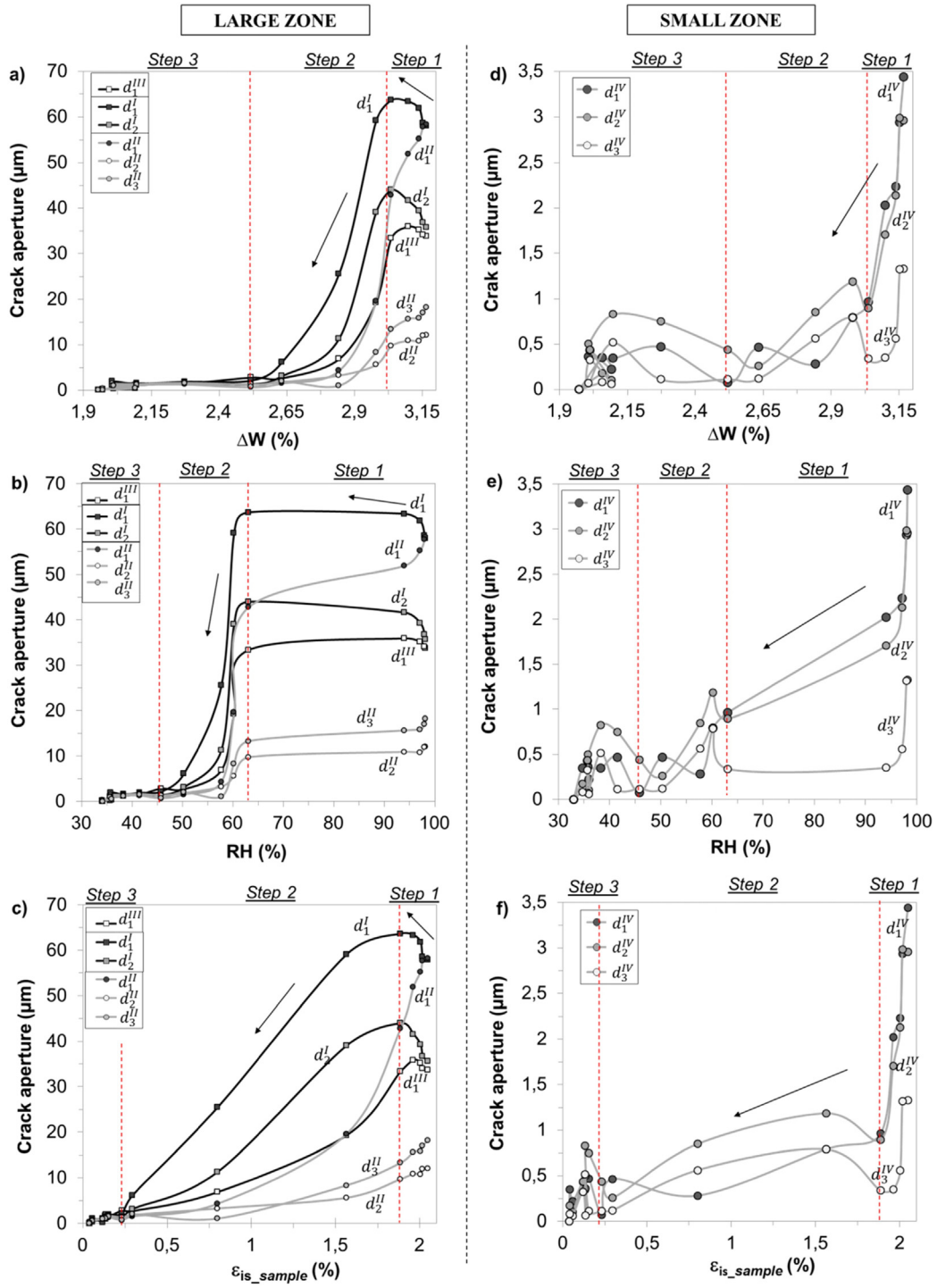

Fig. 6. Crack aperture vs a) averaged water content ΔW, b) RH and c) ε_{is_sample}, for the large zone; crack aperture vs d) ΔW, e) RH and f) ε_{is_sample}, for the small zone.

35 and 63.5 µm). However, significant differences in amplitude were observed, even though the crack apertures of the different types of cracks exhibited similar orders of magnitude.

4.3. Comparison of the desiccation crack apertures vs. RH, ΔW and ε_{is_sample}

The desiccation crack apertures were compared to the RH, average water content (ΔW) and in-plane strain observed at the sample scale (ε_{is_sample}) (Fig. 6). At the end of desiccation (after 10 days of study), at a RH of 33%, the sample was considered dried and stable against deformation and cracking (all of the cracks were closed at the scales studied). Fig. 6 illustrates the behavior of the desiccation cracks at both scales, i.e., the large zone (macroscopic scale) and small zone (mesoscopic scale), and Table 1 summarizes the main features observed in Fig. 6.

In step 1, the type I and III cracks opened, and the type II and IV cracks closed for a short time (≤0.025 day; i.e., ≤40 min). Moreover, the RH variations were high (98% to 63%), whereas the ΔW variations (3.16% to 3.0%) and ε_{is_sample} variations (2.1 to 1.8%) were low. These observations defined shrinkage features on the sample surface, whereas

Please cite this article as: Fauchille, A.-L., et al., Multi-scale study on the deformation and fracture evolution of clay rock sample subjected to desiccation, Appl. Clay Sci. (2016), http://dx.doi.org/10.1016/j.clay.2016.01.054

Table 1
Summary of principal parameter variations and cracking behavior during the desiccation process.

Steps		1 (0.025 day)	2 (0.902 day)	3 (8.98 days)
Observations	ΔW variations	Low 3.17 → 3.03%	High 3.03 → 2.52%	High 2.52 → 1.95%
	RH variations	High 98 → 63%	Medium 63 → 45%	Low 45 → 33%
	ε_{is_sample} variations	Low 2.05 → 1.89%	High 1.89 → 0.23%	Low 0.23 → 0%
	Cracking behaviour	–Crack opening of types I and III –Crack closure of types II and IV	–Crack closure of types I and III –Cracks of types II and IV already closed	All cracks are closed

ε_{is_sample} and ΔW evolved poorly and mainly reflected shrinkage features linked to the whole sample volume.

During step 2, the change in in-plane strain ε_{is_sample} was high (1.8 to 0.25%), and a gradual closure of all cracks was detected and measured. The important changes in the in-plane strain ε_{is_sample} and ΔW between the beginning and end of the second step defined a progressive shrinkage from the surface to the center of the sample.

In step 3, all cracks were closed, but the in-plane strain ε_{is_sample} and ΔW continued to decrease (0.25 to 0%, and 2.52 to 1.96%, respectively). Thus, these values correspond to the sole deformations associated with the clay rock (with no observable crack) at the study scales, in contrast to steps 1 and 2, in which cracks were partially responsible for the measured in-plane strain. Indeed, for steps 1 and 2, the measured sample strain was a complex combination of the clay rock deformation and the strains induced by crack closure or opening.

4.4. Influence of the presence of cracks on the mean in-plane strain values

The mean strain measured at the sample scale (ε_{is_sample}) and the in-plane strains measured in the solid phase (i.e., the clay rock without observable cracks at the macroscopic scale (ε_{is_macro}) and the mesoscopic scale (ε_{is_meso})) were compared during the desiccation path in Fig. 7.

The results indicated that the strain amplitude depended on the study scale. Indeed, ε_{is_meso} measured on the solid phase at the mesoscopic scale was lower than ε_{is_macro}, and ε_{is_macro} was lower than ε_{is_sample}. In the ε_{is_sample} calculation, the cracks on the large zone were all included, and in the ε_{is_macro} calculation, some cracks with an aperture smaller than the camera accuracy were included. At the scales examined, the ε_{is_meso} calculation did not include cracks. Thus, the importance of cracking in the ε_{is_macro} and ε_{is_sample} values was calculated while comparing their maximum values at the beginning of desiccation. The maximum ε_{is_sample} was 2.05%, the maximum ε_{is_macro} was 1%, and the maximum ε_{is_meso} was 0.8%. Therefore, ε_{is_sample} and ε_{is_macro} were overestimated by 61% and 20%, respectively, compared to ε_{is_meso}, which represents the strain of the rock without cracking at the mesoscopic scale. In other words, at the beginning of the test (step 1), 61% of the ε_{is_sample} value and 20% of the ε_{is_macro} value were due to cracking. This result demonstrates the importance of cracking in the deformation calculation at large scale.

In conclusion, the values of ε_{is_macro} overestimated the strains in the solid phase because the closures of small cracks (such as type IV) were detected as strains at the macroscopic scale, and ε_{is_sample} overestimated the in-plane strain of the sample because the opening and closure of the types I, II, III cracks were incorporated in the strain calculations. In our case, the in-plane strain values were dependent on the scale, and the actual in-plane strain of the clay rock between cracks was close to the ε_{is_meso} values.

These results can also be observed in Fig. 8, which represents the evolution of the strains ε_{is_sample}, ε_{is_macro} and ε_{is_meso} as a function of ΔW. Fig. 8 shows that the relationship between the mean strain and ΔW also depends on the investigated scale. Because the unsaturated mechanical behavior of a clay rock is typically described by a constitutive law called the shrinkage curve (Gasc-Barbier and Tessier, 2007), this constitutive relationship may also depend on the study scale as well, particularly when the largest cracks are not accounted for.

5. Discussion: comparison to the gallery scale and microscopic scale

The comparison of the hydromechanical behavior of the Tournemire argillaceous rocks at various scales revealed some similarities and differences, which are summarized in Table 2.

5.1. Types of cracks

In our experiment, regardless of the study scale, sub-horizontal cracks were present, but the distances between these cracks depended on the scale (Table 2). The distance between cracks was up to twenty times greater at the gallery scale than at the macroscopic scale and up to five times greater at the macroscopic scale than at the mesoscopic

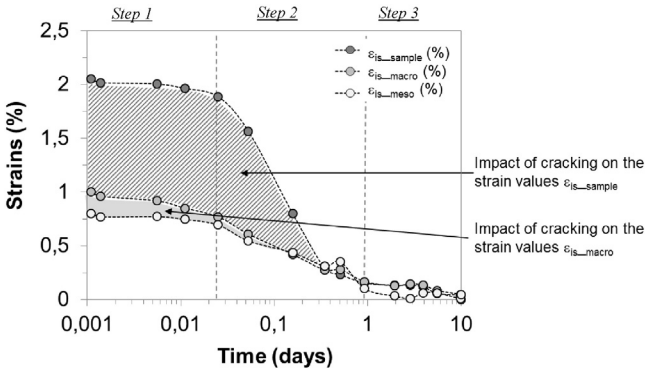

Fig. 7. Mean strains ε_{is_sample}, ε_{is_macro} and ε_{is_meso} vs. time during the desiccation path.

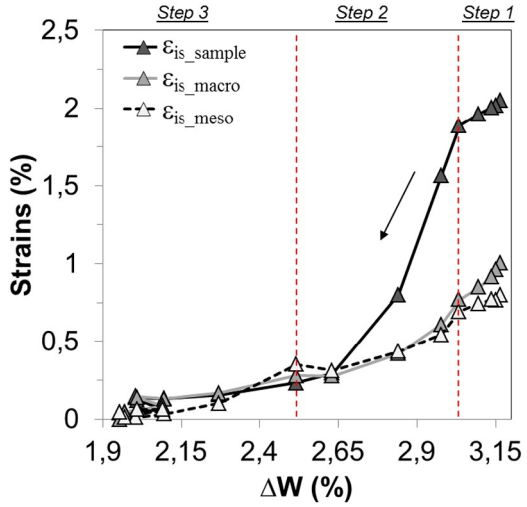

Fig. 8. Mean strains ε_{is_sample}, ε_{is_macro} and ε_{is_meso} vs. averaged water content ΔW.

Please cite this article as: Fauchille, A.-L., et al., Multi-scale study on the deformation and fracture evolution of clay rock sample subjected to desiccation, Appl. Clay Sci. (2016), http://dx.doi.org/10.1016/j.clay.2016.01.054

Table 2
Comparison of the results obtained at different scales.

Observations	Scale				Comments
	Microscopic (μm) (Montes-H et al., 2004; Wang et al., 2013, 2014)	Mesoscopic (mm)	Macroscopic (cm)	Gallery (dm) (Hedan et al., 2014)	
Geometrical patterns of the desiccation cracks	Sub-horizontal cracks Cracks around grains	Sub-horizontal and sub-vertical cracks			–
Strains between the blocks separated by cracks	Heterogeneous strains	No measurable strain	Homogeneous strains	Homogeneous strains	Limitation to a continuous medium
A decrease of HR (98–33%) leads to	Opening and closure of different cracks	Fast opening and then closure of all cracks		Opening of cracks (but cyclic with erratic changes in RH and T)	Different boundary conditions
Maximum crack aperture [μm]	≈1	1.5–3.5	10–60	500	Multi-scale behaviour
Spacing between sub-horizontal cracks [mm]	unkown	0.5–0.9	1–5	64–100	Dependent on the DIC accuracy

scale (Table 2). The quantification of these distances was dependent on the measurement accuracy of the DIC method used to detect the cracks, i.e., it was dependent on the smallest measurable displacement value, which was a fractional value of the elementary pixel used in the optical set-up (approximately 0.1 pixel for H-DIC). The size of this elementary pixel is defined by the dimensions of the study area and the optical parameters of the camera.

Other cracks were observed and designated sub-vertical cracks with variable orientations compared to the sub-horizontal cracks (Fig. 4a and b). The orientation of the sub-vertical cracks with variable orientations exhibited more complex patterns than the sub-horizontal cracks associated with the bedding plane direction (Hedan et al., 2012). At a micrometer scale, Wang et al. (2013, 2014) observed many sub-horizontal cracks on the Callovo-Oxfordian clay rock sample submitted to a desiccation process under ESEM as well as several sub-vertical cracks around coarse grains (e.g., quartz and carbonate). The direction of these micrometer desiccation cracks was more complex and not clearly associated with textural or mineralogical features. At the micrometer scale, the geometric patterns of these cracks might depend on local microstructural heterogeneities in the clay matrix (e.g., small amounts of calcite cements that would have precipitated in the microporosity (Buschaert et al., 2004; Fauchille et al., 2014)).

The crack aperture was ten times greater at the gallery scale than at the macroscopic scale (Table 2). Furthermore, the aperture at the macroscopic scale was ten to twenty times higher than the aperture at the mesoscopic scale. Wang et al. (2013, 2014) and Montes-H et al. (2004) measured mean apertures of 1 μm for various cracks at the micrometer scale in SEM images of deep argillaceous Callovo-Oxfordian rock samples. At these four scales, the measured aperture of the cracks depended on the scale (Table 2).

At different scales (from the microscopic to the gallery), the cracks exhibited dissimilarities, such as the differences in aperture values and distances between two successive cracks. Our observations are consistent with the results of Hedan et al. (2014) and Wang et al. (2013, 2014) and confirmed the multi-scale behavior of crack networks (organization, aperture and distance between cracks) in argillaceous rocks.

5.2. Crack kinematics

The crack closure or opening phenomenon during desiccation in a free condition of deformation and hydric transfer for clay rocks has not been sufficiently observed and quantified in the literature.

The differences between the crack kinematics at the macroscopic and mesoscopic scales cannot be easily explained. However, several experimental studies of clay rocks (Möri et al., 2010) and clay soils (Konrad and Ayad, 1997; Péron et al., 2009) have demonstrated that geometric features, such as the aperture, depth, and spacing of cracks, are strongly interconnected. These studies indicate that the oldest and deepest cracks open more easily than the other cracks; consequently, the crack associated with the highest aperture d_1^l should be the deepest desiccation crack and the first to appear in the studied area at different space scales. However, direct observations of these geometric crack parameters (e.g., width, length, orientation, connectivity, depth) are needed to confirm and clarify these relationships.

At the gallery scale, cracks open when the RH decreases (Hedan et al., 2014). At the microscopic scale, Wang et al. (2013, 2014) observed both crack opening and crack closure when the RH decreased under ESEM. Hallaire (1988) observed a similar phenomenon in natural clay soils at the macroscopic scale. During air-drying desiccation, some cracks opened at the beginning of shrinkage, whereas others closed. These opening and closure phenomena did not induce a volume change and were associated with a clear loss of water in the study samples. Our results at the macroscopic and mesoscopic scales indicated that the cracks closed at the end of the desiccation. This difference in behavior was attributed to the boundary conditions. In our laboratory study, all sample faces were free of deformation and drained (water mass can transfer through most of the surface of the study sample). By contrast, in the in situ case, only the front gallery was free of deformation; in the micrometer case, one face did not have any contact with air in the ESEM. These observations indicate that the opening and closing of cracks is related to desiccation and hydration in a complex manner: there is a non-bijective relationship between these features that also accounts for the hydric and mechanical conditions at the boundary of the sample (free or constrained condition).

At the macroscopic scale (i.e., on the large zone in Fig. 2) and the gallery scale (Hedan et al., 2014), homogeneous strains perpendicular to the stratification were observed (Fig. 4). However, the values accounted for the closure and opening of desiccation cracks: they cannot be considered as pure hydro-mechanical strains occurring with no fracturing processes.

6. Conclusions

A non-invasive DIC method was used on an argillaceous rock sample subjected to a desiccation process under measured and controlled RH and temperature. A new experimental set-up was designed to investigate the kinematic fields and patterns (displacement, strains, crack opening and closure) at two scales: mesoscopic (millimeter) and macroscopic (centimeter). This experimental laboratory investigation permitted the monitoring of deformations at both scales for (a) the spatial clay rock deformations and (b) the crack evolution (opening and closure) to calculate their aperture during desiccation.

From a phenomenological perspective, several conclusions have been reached. As observed in the Tournemire site (crack aperture ≤ 500 μm), our laboratory work demonstrated that hydric changes induce sub-horizontal cracks and sub-vertical cracks whose apertures were between 3.5 and 63.5 μm. At the beginning of the desiccation (<0.025 days, i.e., <40 min), some cracks opened

Please cite this article as: Fauchille, A.-L., et al., Multi-scale study on the deformation and fracture evolution of clay rock sample subjected to desiccation, Appl. Clay Sci. (2016), http://dx.doi.org/10.1016/j.clay.2016.01.054

rapidly, whereas other cracks closed. One half day after the data acquisition began, all of the desiccation cracks were closed; the desiccation process induced the closure of all cracks under free deformation and drained conditions. Under free deformation conditions, our observations suggest shrinkage from the surface to the center of the sample. Moreover, the comparison between the crack apertures and the distance between cracks at four scales (from the microscopic to the gallery scale) reveals they are multiscale parameters of clay rocks. The crack kinematics also exhibited multiscale behavior from the microscopic scale to the gallery scale, but this behavior appeared to depend on boundary conditions.

With respect to the relationship between strains and cracking, this study highlights that the crack apertures and the mean strain representing the "volumetric" strain were clearly correlated to RH and ΔW changes in the waterproof box. Furthermore, according to the considered scale, 20% of the mean strain ε_{is_macro} values and 61% of the mean strain ε_{is_sample} values were due to the presence of cracking. Thus, these mean strains were greatly overestimated.

The interpretation of the entire dataset has emphasized two aspects. First, the concept of strain in the context of desiccation cracking is scale dependent. Second, our results suggest that a multi-scale approach is required to understand desiccation cracking mechanisms in clay rocks. In other words, the evolution of the kinematic fields and patterns (apertures, spacing, depths of desiccation cracks and hydric strains) induced by desiccation can be understood at different scales if their measurements, their characterization and their corresponding physico-mechanical processes (micro-cracking induced by drying and wetting) are considered simultaneously.

Acknowledgments

The authors acknowledge the NEEDS-MIPOR program (Nucléaire, Energie, Environnement, Déchets, Société-MIlieux POReux) and the French Institute for Nuclear Safety and Radioprotection (IRSN) for supporting and funding this work. The authors are also grateful to M. Pascal Touvenet, M. Pascal Rogeon, M. Claude Laforest, M. Frédéric Limousin and Mrs. Alice Coffey for technical assistance.

References

Bésuelle, P., Viggiani, G., Desrues, J., Bornert, M., 2006. X-ray micro CT for studying strain localization in clay rocks under triaxial compression. Advances in X-ray Tomography for Geomaterials. ISTE Ltd., London, pp. 35–52.

Blüming, P., Bernier, F., Lebon, P., Martin, C.D., 2007. The excavation-damaged zone in clay formations — time-dependent behaviour and influence on performance assessment. Phys. Chem. Earth 32, 588–599.

Bonin, B., 1998. Deep geological disposal in argillaceous formations: studies at the tournemire test site. J. Contam. Hydrol. 35, 315–330.

Bornert, M., Valès, F., Gharbi, D., Nguyen Minh, D., 2010. Multiscale full-field strain measurements for micromechanical investigation of the hydromechanical behaviour of clayey rocks. Strain 46 (1), 33–46.

Bossard, P., Meier, M.P., Moeri, A., Trick, T., Major, J.C., 2002. Geological and hydraulic characterisation of the excavation disturbed zone in the Opalinus clay of the Mont Terri Rock Laboratory. Eng. Geol. 66 (1–2), 19–38.

Bruck, H., McNeill, S., Sutton, M., Peters, W., 1989. Digital image correlation using Newton–Raphson method of partial differential correction. Exp. Mech. 29, 261–267.

Buschaert, S., Fourcade, S., Cathelineau, M., Deloule, E., Martineau, F., Ougougdal, M.A., Trouiller, A., 2004. Widespread cementation induced by inflow of continental water in the eastern part of the Paris basin: O and C isotopic study of carbonate cements. Appl. Geochem. 19 (8), 1201–1215.

Cabrera, J., Beaucaire, C., Bruno, G., De Windt, L., Genty, A., Ramambasoa, N., Rejeb, A., Savoye, S., Volant, P., 2001. Projet Tournemire: Synthèse des Résultats des Programmes de Recherche 1995/1999. IRSN Report.

Charpentier, D., Mosser-Ruck, R., Cathelineau, M., Guillaume, D., 2004. Oxidation of mudstone in a tunnel (Tournemire, France): consequences for the mineralogy and chemistry of clays minerals. Clay Miner. 39, 135–149.

Constantin, J., Vergely, P., Cabrera, J., 2002. Tectonique et fracturation associée dans le bassin des Causses (Aveyron, France): le cas du secteur de Tournemire (Aveyron, France). Bull. Soc. Géol. Fr. 173, 229–243.

Cosenza, P., Ghoreychi, M., de Marsily, G., Vasseur, G., Violette, S., 2002. Theoretical prediction of poroelastic properties of argillaceous rocks from *in situ* specific storage coefficient. Water Resour. Res. 38 (10), 25-1–25-12.

De Windt, L., Cabrera, J., Boisson, J.Y., 1998. Hydrochemistry in an indurated Argillaceous Formation (Tournemire Tunnel Site, France). In: Arehart, Hulsto (Eds.), Water–Rock Interaction. Balkema, Rotterdam, pp. 145–148.

Desrues, J., Lanier, J., Stutz, P., 1985. Localization of the deformation in tests on sand sample. Eng. Fract. Mech. 21 (4), 909–921.

Fauchille, A.L., 2015. Déterminismes microstructuraux et minéralogiques de la fissuration hydrique dans les argilites de Tournemire: apports couples de la pétrographie quantitative et de la correlation d'images numériques (PhD thesis of) Poitiers University, France.

Fauchille, A.L., Hedan, S., Prêt, D., Valle, V., Cabrera, J., Cosenza, P., 2014. Relationships between desiccation cracking behavior and microstructure of the Tournemire clay rock by coupling DIC and SEM methods. Proceedings of IS-Cambridge, Geomechanics from Micro to Macro 1–3 Sept. 2014 2, pp. 1421–1424.

Gasc-Barbier, M., Tessier, D., 2007. Structural modifications of a hard deep clayey rock due to hygro-mechanical solicitations. Int. J. Geomech. 7 (3), 227–235.

Grégoire, D., Maigre, H., Morestin, F., 2009. New experimental techniques for dynamic crack localization. Eur. J. Comput. Mech. 18 (3–4), 255–283.

Hallaire, V., 1988. La fissuration d'un sol argileux au cours du dessèchement I, description in situ. Agronomie 8-2, 139–145.

Hedan, S., Cosenza, P., Valle, V., Fauchille, A.L., Dudoignon, P., Cabrera, J., 2012. Investigation of the damage induced by desiccation and heating of Tournemire argillite using digital image correlation. Int. J. Rock Mech. Min. Sci. 51, 64–75.

Hedan, S., Fauchille, A.L., Valle, V., Cabrera, J., Cosenza, P., 2014. One-year monitoring of desiccation cracks in Tournemire argillite using digital image correlation. Int. J. Rock Mech. Min. Sci. 68, 22–35.

Jin, H., Bruck, H.A., 2005. Pointwise digital image correlation using genetic algorithms. Exp. Tech. 291, 36–39.

Konrad, J.M., Ayad, R., 1997. Desiccation of as sensitive clay: field experimental observations. Can. Geotech. J. 34, 929–942.

Lenoir, N., Bornert, M., Desrues, J., Viggiani, G., 2007. 3D digital image correlation applied to X-ray micro tomography from triaxial compression tests on argillaceous rock. Strain 43, 193–205.

Matray, J.M., Savoye, S., Cabrera, J., 2007. Desaturation and structure relationships around drifts excavated in the well-compacted Tournemire's argillite (Aveyron, France). Eng. Geol. 90, 1–16.

Montes-H, H.G., Duplay, J., Martinez, L., Escoffier, S., Rousset, D., 2004. Structural modifications of Callovo-Oxfordian argillite under hydration/dehydration conditions. Appl. Clay Sci. 25, 187–194.

Möri, A., Bossart, P., Matray, J.M., Franck, E., Fatmi, H., Ababou, R., 2010. Mont Terri Project: cyclic deformations in the Opalinus clay. Proceedings of the International Meeting of Clay in Natural and Engineered Barriers for Radioactive Waste Confinements, Nantes 29 March-01 April 2010, pp. 103–124.

Niandou, H., Shao, J.F., Henry, J.P., Fourmaintraux, D., 1997. Laboratory investigation of the mechanical behaviour of Tournemire shale. Int. J. Rock Mech. Min. Sci. 34, 3–16.

Okay, G., Cosenza, P., Ghorbani, A., Camerlynck, C., Cabrera, J., Florsch, N., Revil, A., 2013. Localization and characterization of cracks in clay rocks using frequency and time-domain induced polarization. Geophys. Prospect. 61 (1), 134–152.

Péron, H., Hueckel, T., Laloui, L., Hu, L.B., 2009. Fudamentals of desiccation cracking of fine-grained soils: experimental characterisation and mechanisms identification. Can. Geotech. J. 46, 1177–1201.

Réthoré, J., Hild, F., Roux, S., 2008. Extended digital image correlation with crack shape optimization. Int. J. Numer. Methods Eng. 73 (2), 248–272.

Robinet, J.-C., 2008. Minéralogie, porosité et diffusion de solutés dans l'argilite du Callovo-Oxfordien de Bure (Meuse/Haute-Marne, France) de l'échelle centimétrique à millimétrique (Thèse de doctorat de l'Université de Poitiers).

Rotinat, R., Tie Bi, R., Valle, V., Dupre, J.C., 2001. Three optical procedures for local large-strain measurement. Strain 37 (3), 89–98.

Sutton, M.A., Wolters, W.J., Peters, W.H., Ranson, W.F., McNeill, S.R., 1983. Determination of displacements using an improved digital image correlation method. Image Vis. Comput. 1 (3), 133–139.

Tremosa, J., Arcos, D., Matray, J., Bensenouci, F., Gaucher, E., Tournassat, C., Hadi, J., 2012. Geochemical characterization and modelling of the Toarcian/Domerian porewater at the Tournemire underground research laboratory. Appl. Geochem. 27 (7), 1417–1431.

Tsang, C.F., Bernier, F., Davies, C., 2005. Geohydromechanical processes in the excavation damaged zone in crystalline rock, rock salt, and indurated and plastic clays - In the context of radioactive waste disposal. Int. J. Rock Mech. Min. Sci. 42 (1), 109–125.

Valès, F., 2008. Modes de déformation et d'endommagement des roches argileuses profondes sous sollicitations hydro-mécaniques (Ph-D Thesis) Ecole Polytechnique, Palaiseau (France).

Valès, F., Nguyen Minh, D., Gharbi, H., Rejeb, A., 2004. Experimental study of the influence of the degree of saturation on physical and mechanical properties in Tournemire shale (France). Appl. Clay Sci. 26, 197–207.

Valle, V., Hedan, S., Cosenza, P., Berdjane, M., Fauchille, A.-L., 2015. Digital image correlation development for the study of materials including multiple crossing cracks. Exp. Mech. 55, 379–391.

Wang, L., 2012. Micromechanical Experimental Investigation and Modeling of Strain and Damage of Argillaceous Rocks Under Combined Hydric and Mechanical Loads (Ph-D Thesis) Ecole Polytechnique, Palaiseau (France).

Wang, L., Bornert, M., Chanchole, S., Yang, D.S., Héripré, E., Tanguy, A., Caldemaison, D., 2013. Microscale experimental investigation of the swelling anisotropy of the Callovo-Oxfordian argillaceous rock. Clay Miner. 48, 391–402.

Wang, L., Bornert, M., Héripré, E., Yang, D.S., Chanchole, S., 2014. Irreversible deformation and damage in argillaceous rocks induced by wetting and drying. J. Appl. Geophys. 107, 108–118.

Yang, D., Bornert, M., Chanchole, S., Wang, L., Valli, P., Gatmiri, B., 2011. Experimental investigation of the delayed behavior of unsaturated argillaceous rocks by means of digital image correlation techniques. Appl. Clay Sci. 54, 53–62.

Please cite this article as: Fauchille, A.-L., et al., Multi-scale study on the deformation and fracture evolution of clay rock sample subjected to desiccation, Appl. Clay Sci. (2016), http://dx.doi.org/10.1016/j.clay.2016.01.054